Videometric water surface tracking of spatial impulse wave propagation

Author(s):
Evers, Frederic M.

Publication date:
2018-12

Permanent link:
https://doi.org/10.3929/ethz-b-000307564

Originally published in:
Journal of visualization 21(6), https://doi.org/10.1007/s12650-018-0507-1

Funding acknowledgement:
143657 - Spatial impulse waves (SNF)

This is a post-peer-review, pre-copyedit version of an article published in Journal of Visualization. The final authenticated version is available online at: https://doi.org/10.1007/s12650-018-0507-1

Videometric water surface tracking of spatial impulse wave propagation

Frederic M. Evers[1]

[1] Postdoctoral Researcher, Laboratory of Hydraulics Hydrology and Glaciology (VAW), ETH Zurich, CH-8093 Zürich, Switzerland, evers@vaw.baug.ethz.ch, ORCID 0000-0001-5181-8978 (corresponding author)

Keywords: Impulse wave; Landslide; Physical modelling; Videometry; Water surface tracking

Introduction

Gravity-driven mass movements, e.g. landslides or avalanches, may generate large water waves in oceans and inland waters including lakes and reservoirs (Heller *et al*. 2009). The generation mechanism of these so-called impulse waves involves a momentum transfer from the slide mass to the water body. The impulse waves generated by a rockslide at Lituya Bay, USA, in 1958 caused runup heights of more than 500 m (Miller 1960). Recent events include Chehalis Lake, Canada, in 2007 (Roberts *et al.* 2013), Taan Fjord, USA, in 2015 (George *et al.* 2017), and Karat Fjord, Greenland, in 2017 (Gauthier *et al.* 2018). Due to the complex wave generation processes, hydraulic experimentation is a major research method to improve the understanding of these events. Empirical equations derived from these experiments apply for hazard assessments at prototype scale to predict wave magnitudes (Heller *et al*. 2009). Di Risio *et al.* (2011) discuss experimental studies both for unidirectional wave propagation in a wave channel (2D) and for omnidirectional wave propagation in a wave basin (3D). In 2D, the standard measuring approach with wave gauges at discrete locations may be complemented with tracking the meniscus of the free water surface at a glass side wall to obtain a continuous representation (Viroulet *et al.* 2013). However, in 3D, water surface contours are not traceable in such a straightforward manner and discrete wave gauges only yield data at a few scattered locations. In addition, physical scale models of impulse wave generation and propagation require sufficient model dimensions with still water depth $h \geq 0.2$ m to avoid significant scale effects (Heller *et al.* 2008), which places additional demands on the instrumentation. Therefore, a videometric measurement system was applied to visualize and track the spatial and temporal evolutions of the free water surface. The prospects of videometry for visualizing and investigating spatial impulse wave propagation are presented in this work.

Experimental setup

The impulse waves were generated in a 4.5 m by 8 m wave basin with a chute featuring a release box on an inclinable sliding plane (Fig. 1). The chute allowed for adjusting the slide impact angle α between 30° and 90°. The slides were accelerated by gravity after manual release from the box at different drop heights. The slide impact velocity V_s was measured with laser light barriers mounted perpendicular to the sliding plane. The granular slide material had bulk density ρ_s = 1338 kg/m^3. A ProSurf-system (AICON 3D Systems GmbH, Braunschweig, Germany) with four cameras was positioned around one half of the wave basin. Deionized water in the basin was dyed white with titanium dioxide (TiO_2) pigments (KRONOS 1002, KRONOS Worldwide, Inc., Dallas, USA) at a mass concentration of 4 kg/m^3. The addition of TiO_2 had negligible effects on the water viscosity and the surface tension (Przadka *et al.* 2012). The white and opaque water surface allowed for projecting a regular grid pattern with 79 × 79 intersections in the center of the four cameras. This grid projection defined the measurement zone covering slightly more than half of the full radial wave pattern (Fig. 1). The grid spacing was approximately 4 cm depending on the throw, i.e. the distance between the projector and the free water surface. The grid spacing was set sufficiently large to achieve a reliable greyscale-based pattern recognition of the camera data. The four ProSurf-cameras were synchronized by a control box to an acquisition rate of 24 Hz. Their position and orientation was calibrated, enabling the spatial tracking of the grid intersection by triangulation, yielding a point cloud representing the free water surface (Evers and Hager 2015, Evers 2017). An additional side camera was positioned diagonally opposite to the slide impact location. Evers (2017) provides additional details on the experimental setup.

This is a post-peer-review, pre-copyedit version of an article published in Journal of Visualization. The final authenticated version is available online at: https://doi.org/10.1007/s12650-018-0507-1

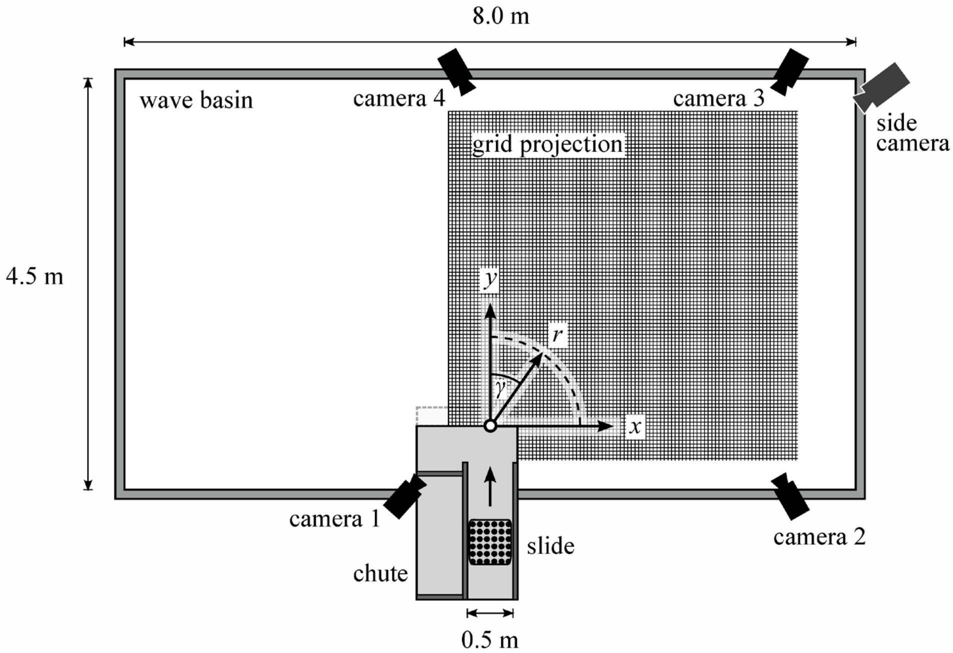

Fig. 1 Experimental setup of 3D wave basin

Measured water surface contours

Fig. 2 shows the oblique views of the side camera as well as the water surface contours at different times t for a selected test run. The contour plots were generated from the point cloud of the measured grid intersections by bicubic interpolation. The impacting slide mass features a slide centroid velocity V_s = 4.35 m/s, a slide mass m_s = 20 kg, a slide thickness s = 0.12 m, a slide width b = 0.50 m, and a slide impact angle α = 60°. The still water level is set to h = 0.3 m. In Fig. 2(a) at t = 0.00 s, the instant of time before impact is shown with a plane water surface. At t = 0.21 s in Fig. 2(b), the slide mass has impacted the water creating a splash screen with an impact crater behind. The contour plot reproduces the uplifting of the water surface. The impact crater collapses at t = 0.50 s (Fig. 2(c)) and the first wave crest emerges from the slide impact zone. While the first wave crest is barely visible in the side camera image, it may be well distinguished in the vertically exaggerated contour plot. At t = 0.96 s (Fig. 2(d)), the first wave trough emerges. A steeper second wave crest has formed and propagates away from the impact zone between t = 1.46 s and 1.92 s (Fig. 2(e)-(f)). In Fig. 3 water surface profiles extracted from contour plots in Fig. 2 are shown. Although momentary minor gaps may occur, e.g. at t = 0.96 s for wave propagation angle γ = 0°, the quasi-continuous water surface profiles yield insights similar to side window images of a 2D wave channel.

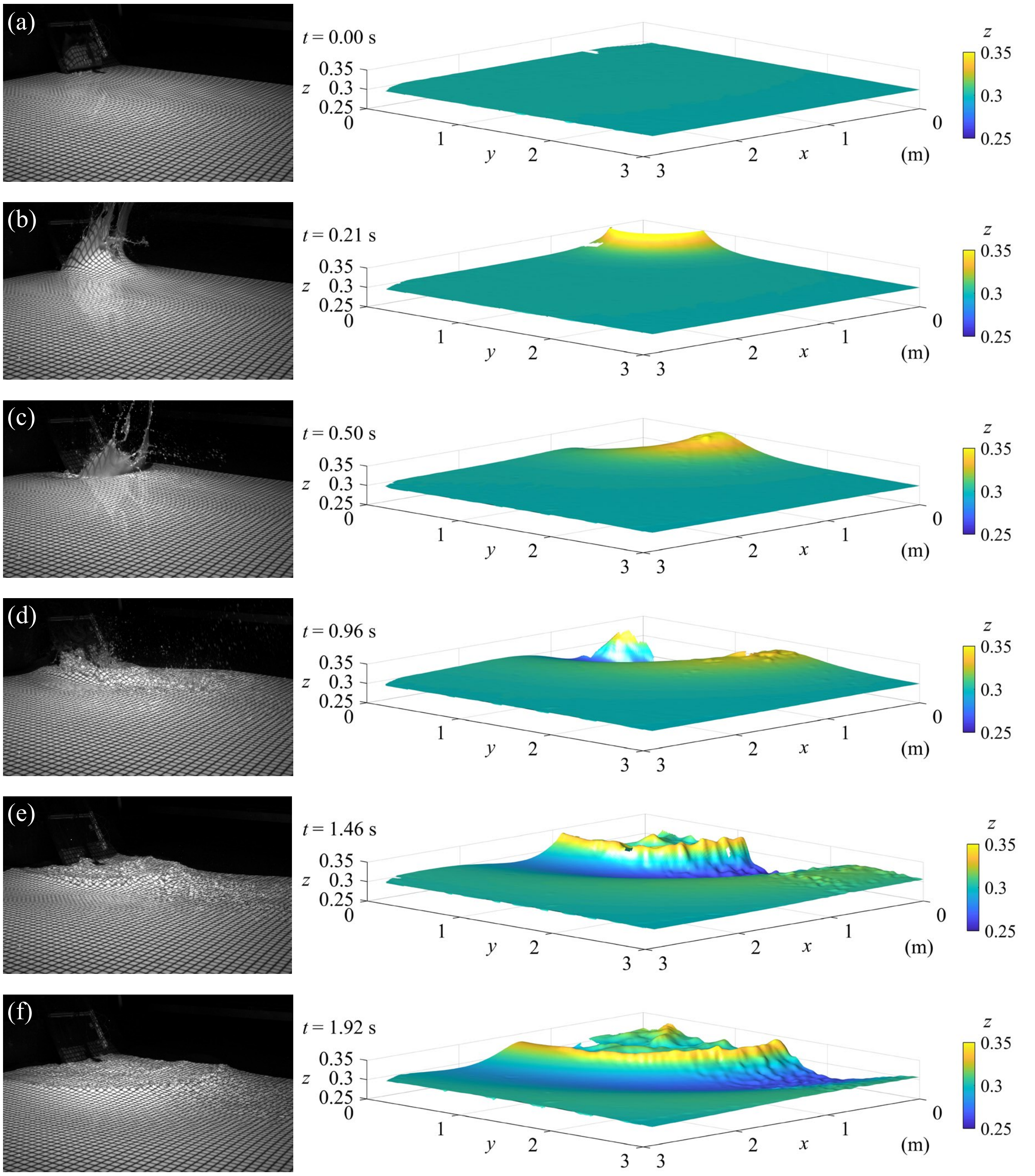

Fig. 2 Side camera images (left) and interpolated 3D contour plots of the water surface (right) for V_s = 4.35 m/s, m_s = 20 kg, s = 0.12 m, b = 0.50 m, and α = 60° at different times

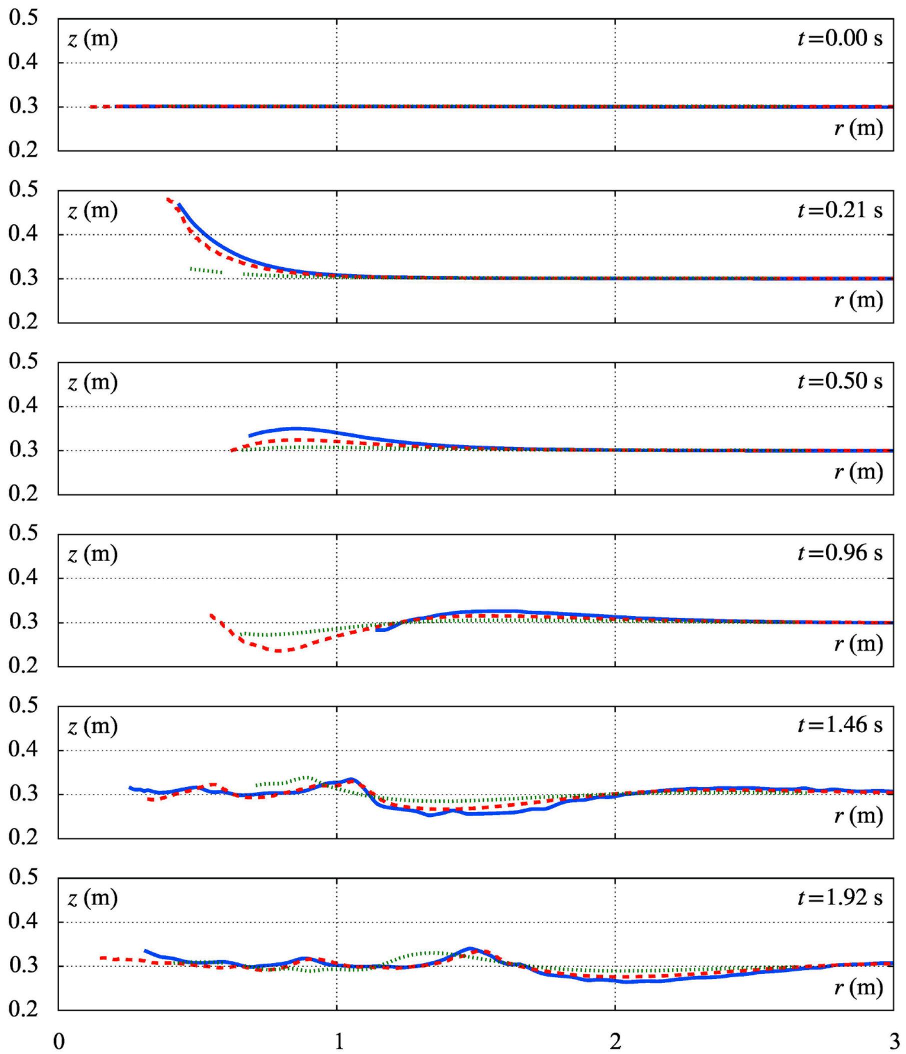

Fig. 3 Extracted water surface profiles for V_s = 4.35 m/s, m_s = 20 kg, s = 0.12 m, b = 0.50 m, and α = 60° at γ = 0° (—), 45° (– –), and 90° (····) at different times

Conclusions

Spatial impulse wave propagation in a laboratory wave basin was measured with a videometric technique by tracking a projected grid pattern on the free water surface. On the one hand, the grid spacing has to be sufficiently large to achieve a reliable pattern recognition, on the other hand it has to be small enough to resolve essential impulse wave features. The interpolated contour plots and water surface profiles show that the resolution of the videometric measurement system is sufficient for this task. Therefore, the application of videometry enables an in-depth phenomenological description and quantification of spatial impulse wave generation and propagation processes. Evers (2017) applied this technique to an extensive test program and provides a quantitative analysis of key wave characteristics as a function of the governing slide impact parameters.

Acknowledgments

This work was supported by the Swiss National Science Foundation (Project No. 200021-143657) and is part of the Swiss Competence Center for Energy Research – Supply of Electricity (SCCER-SoE).

Notation

b	Slide width (m)
h	Still water depth (m)

m_s	Slide mass (kg)
r	Radial wave propagation distance (m)
s	Slide thickness (m)
t	Time (s)
V_s	Slide centroid velocity (m s^{-1})
x	x-coordinate (m)
y	y-coordinate (m)
z	z-coordinate (m)
α	Slide impact angle (°)
γ	Wave propagation angle (°)
ρ_s	Bulk slide density (kg m^{-3})

References

Di Risio, M.; De Girolamo, P.; Beltrani, G. M. (2011). Forecasting Landslide Generated Tsunamis: a Review: 81–106, N.-A. Mörner ed. *The Tsunami Threat - Research and Technology*. InTech. doi:10.5772/13767

Evers, F. M. (2017). Spatial propagation of landslide generated impulse waves. *Doctoral Dissertation* No 24650 and *VAW-Mitteilung* 244 (R. Boes, ed.), ETH Zurich, Zürich. doi:10.3929/ethz-b-000209471

Evers, F. M.; Hager, W. H. (2015). Videometric water surface tracking: towards investigating spatial impulse waves. Proc. 36th *IAHR Congress*, The Hague. doi:10.3929/ethz-a-010630706

Gauthier, D.; Anderson, S. A.; Fritz, H. M.; Giachetti, T. (2018). Karrat Fjord (Greenland) tsunamigenic landslide of 17 June 2017: initial 3D observations. *Landslides*, 15(2), 327–332. doi: 10.1007/s10346-017-0926-4

George, D. L.; Iverson, R. M.; Cannon, C. M. (2017). New methodology for computing tsunami generation by subaerial landslides: Application to the 2015 Tyndall Glacier landslide, Alaska. *Geophys. Res. Lett.*, 44, 7276–7284. doi:10.1002/2017GL074341

Heller, V.; Hager, W. H.; Minor H.-E. (2008) Scale effects in subaerial landslide generated impulse waves. *Exp. Fluids*, 44(5), 691–703. doi:10.1007/s00348-007-0427-7

Heller, V.; Hager W. H.; Minor, H.-E. (2009). Landslide generated impulse waves in reservoirs: Basics and computation. *VAW-Mitteilung* 211, H.-E. Minor, ed. ETH Zurich, Zürich.

Miller, D. J. (1960). The Alaska earthquake of July 10, 1958: giant wave in Lituya Bay. *Bulletin of the Seismological Society of America*, 50(2), 253–266.

Przadka, A.; Cabane, B.; Pagneux, V.; Maurel, A.; Petitjeans, P. (2012). Fourier transform profilometry for water waves: how to achieve clean water attenuation with diffusive reflection at the water surface?. *Exp. fluids*, 52(2), 519-527. doi:10.1007/s00348-011-1240-x

Roberts, N.J.; McKillop, R.J.; Lawrence, M.S.; Psutka, J.F.; Clague, J.J.; Brideau, M.A.; Ward, B.C. (2013). Impacts of the 2007 landslide-generated tsunami in Chehalis Lake, Canada. *Landslide Science and Practice 6* (C. Margottini; P. Canuti; K. Sassa, eds.). 133-140. doi:10.1007/978-3-642-31319-6_19

Viroulet, S.; Sauret, A.; Kimmoun, O.; Kharif, C. (2013). Granular collapse into water: toward tsunami landslides. *Journal of Visualization*, 16, 189–191. doi:10.1007/s12650-013-0171-4